

Effects of reflections on TE-wave measurements of electron cloud density *

K. Hammond, Harvard University, Cambridge MA,
 J. Sikora, K. G. Sonnad[†] CLASSE, Cornell University, Ithaca NY,
 S. Veitzer, TechX Corp, Boulder CO

Abstract

The TE-wave transmission technique is a method for measuring the electron cloud (EC) density in an accelerator beam pipe. It involves transmitting an RF signal through the pipe and detecting the intensity of the phase modulation caused by the fluctuating EC density. Using physical and simulated data, the experiments described in this paper explore the effects of reflections on the phase advance of TE-waves. It is shown that introducing reflections to a waveguide can significantly distort phase measurements in some cases.

INTRODUCTION

This paper focuses on the TE-wave transmission method for determining Electron Cloud (EC) density. This method, first proposed for the SPS at CERN [1, 2], involves using beam position monitor (BPM) buttons to transmit electromagnetic waves at microwave-range frequencies through a length of beam pipe. The method later was demonstrated to work at the SLAC PEP II Low Energy Ring by using solenoid field setting to control the electron cloud density. [3] We explore the influence of internal reflections within the beam pipe on these measurements. Accelerator beam pipes are far from ideal waveguides, and the EC is not the only perturbation that the TE-waves encounter. Numerous measurement instruments alter the beam pipe walls, and the overall dimensions of the pipe change periodically as the beam passes through different regions of CESR. Such effects are likely to cause reflections and, possibly, resonances. If some waves reflect between two protrusions one or more times before reaching a detector, they will undergo a greater phase advance than those that transmit without reflection. Under such circumstances, phase shift measurements would not accurately represent the EC if reflections are ignored. The experiments and simulations described in the following sections were intended to help elucidate the effects of reflections on guided waves in accelerator beam pipes.

EXPERIMENTAL SETUP

The effects of nonuniformities on TE-wave transmission were studied with physical waveguides and with numerical

simulation software.

Physical Model

The physical waveguides were copper pipes with rectangular cross sections. The pipes had flanges affixed to each end, allowing for pipes to be connected to one another to increase overall length. Transverse dimensions were 0.072m x 0.034m; pipe lengths were on the order of one meter. On some occasions, washers were added between flanges at the junction of two lengths of pipe to allow an opening for the introduction of nonuniformities such as metal strips or Lexan plastic. The presence of the narrow (~ 0.002 m) space between adjoined pipes itself had no noticeable effect on the TE-wave signal.

TE-wave signals were generated and recorded with an Aeroflex 3281A spectrum analyzer for some experiments and a Hewlett Packard 8753B network analyzer for others. The signal reached the waveguide through a coaxial cable with a characteristic impedance of 50Ω , and was transmitted to the pipe through an antenna. A receiving antenna picked up the signal at the other end, returning the signal to the generator through a similar cable that terminated at a 50Ω resistor. The signal generator repeatedly swept through a specified frequency range (less than 3 GHz) with a sampling period on the order of tens of microseconds. Signal intensity was about -20 dBm.

Simulation

VORPAL, a particle-in-cell plasma simulation code [4], was used for the numerical models described in this paper. VORPAL software maps three-dimensional space onto a grid, assigning values for physical quantities such as EM field components to each set of coordinates. Boundary conditions, as well as physical attributes such as current density, may be programmed directly into the simulation code. Yee's algorithm [5] was employed in these simulations to solve Maxwell's equations for the coordinates at each time step. Particle positions and velocities were updated using the relativistic Boris algorithm [6].

The boundary conditions used for these simulations were characterized by two types of cross-sectional geometry and two types of end behavior. The cross-sections were either those of the rectangular pipe described above or of the CESR beampipe. The latter consists of two circular arcs (radius 0.075m) connected with flat side planes. It is about 0.090m from side to side and 0.050m between the apices

* Work supported by NSF grants PHY-0849885 and PHY-0734867 and DOE grant DE-FC02-08ER41538

[†] kgs52@cornell.edu

of the arcs. For both cross-sections, VORPAL constrained the values of the parallel electric field components to zero (the boundary conditions for a perfect conductor).

The ends of the pipes were either perfect conductors or perfectly-matched layers (PMLs) designed to fully absorb any transmissions. Applying the conducting boundaries created a resonant cavity; using PMLs simulated a section of a longer, continuous beam pipe. PML boundaries, first developed by J. Berenger [7], ascribe a parabolically increasing electrical and (nonphysical) magnetic conductivity to the regions at the ends of the beam pipes. These regions had significant thickness, sometimes as much as one-fourth the length of the entire pipe.

VORPAL maintains an electron cloud by generating a specified initial distribution of particles in the simulation grid and tracking their subsequent motion due to field interactions. The simulation uses macroparticles of high mass and charge to represent groups of nearby electrons. Cells on the boundary of the EC region are made to delete particles that pass through them to prevent the particles from escaping. Secondary particle sources (such as metallic surfaces) are also available, but none were used in these tests. Instead, electrons were set to initially have zero velocity (a cold plasma). They were also artificially constrained to cross no more than one cell per time step, a restriction that in practice has does not significantly limit the physicality of the simulation.

Waves were excited in the simulations by ascribing a transverse-direction current density to a section of the beam pipe. These sections covered the full cross-sectional area and were two cells thick in the longitudinal dimension.

In addition to recording all EM field data at user-specified intervals, VORPAL can record the time evolution of a number of different quantities over the entire simulation. Known in the code as Histories, recordable quantities include the potential difference between two given points, energy flux through a specified cross section, and the number of particles in a given region. The energy flux history is especially useful for testing the effectiveness of the PML boundaries, since all flux is expected to point away from the source current in the absence of reflections.

One aspect of the simulation that is very different from the actual TE-wave measurements both in the rectangular pipe and the beam pipe is the time scale. While the physical measurements occurred over arbitrarily long periods of time during which the received signals were steady, the simulations modeled systems over periods no longer than one to two hundred nanoseconds. Simulations longer than that tended to exhibit roundoff error, with all field component values increasing exponentially without bound.

RESONANT CAVITY MEASUREMENTS

The resonant cavity experiments conducted with the physical beam pipe and the simulations accomplished two main objectives: to test the accuracy of the simulations and to determine a cutoff frequency for the CESR beam pipe,

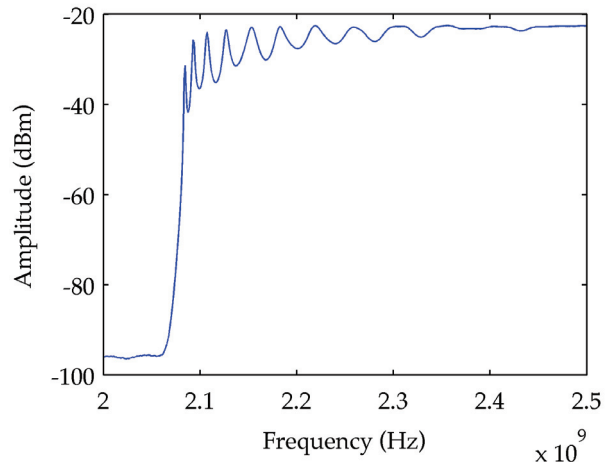


Figure 1: The frequency domain of a 1.219m pipe with a cutoff frequency of approximately 2.08 GHz. Reflections, whose presence is indicated by the resonant frequency peaks, arose because the receiving antenna could not fully absorb the signal.

which would be difficult to derive analytically due to its geometry.

The resonant frequencies of a cavity are those for which the pipe length is a multiple of the half-wavelength. The wavelength λ of a given frequency f (in Hz) in a guide with cutoff frequency f_c can be found from the phase velocity

$$v_\phi = \frac{cf}{\sqrt{f^2 - f_c^2}}, \quad (1)$$

which arises directly from the dispersion relation (Eq. 1) for an empty pipe. The resonant wavelengths must satisfy

$$\lambda = \frac{v_\phi}{f} = \frac{2L}{n}, \quad (2)$$

where L is the pipe length and n is an integer. Consequently, the frequency of the n th resonant harmonic satisfies the hyperbolic relationship

$$f^2 = \frac{c^2}{4L^2}n^2 + f_c^2. \quad (3)$$

The spectrum analysis for a 1.219m rectangular pipe (Fig. 1) showed a series of peaks in the frequency domain in agreement with Eq. 9.

Simulating the frequency sweep used to produce the distribution function in Fig. 1 would not be practical due to the limited time frame and discrete time steps. However, transmitting a single frequency will still produce a full distribution in the frequency domain because the signal is effectively a pulse in the time scale of the simulation. Although the carrier frequency's magnitude in the distribution is at least 10dBm stronger than that of any other frequency and much greater if the carrier resonates, the peaks representing the harmonics are still clearly visible (see Fig. 2).

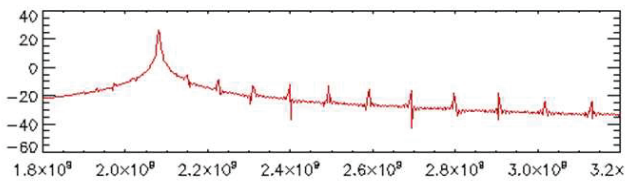


Figure 2: The distribution function from the VORPAL simulation for a 1m resonant cavity. The greatest peak is at the carrier frequency (2.081GHz, which is also a resonant harmonic). Note that other peaks at resonant frequencies are clearly visible.

The locations of the peaks in the simulation’s frequency domain tended to suggest a cavity length greater than the programmed length of 1.219m. Increasing the number of grid points per unit distance improved the accuracy of the peak locations, and the suggested length was accurate within 0.5% when the longitudinal distance between grid points was ≤ 1 cm. It was also noted that the peaks in the Fourier transform did not obey the hyperbolic relationship (Eq. 9) indefinitely. For frequencies past 9 GHz the spacing between the peaks began to decrease, and no peaks were visible for frequencies greater than 12 GHz. This is to be expected, because at high frequencies the wavelength λ falls to a level comparable with the grid point spacing and thus precludes an accurate simulation.

With some confidence established in the accuracy of the simulated frequency peak data, the simulation could then be used to produce an estimate of the CESR beam pipe cutoff frequency. The locations of the first twenty-one frequency peaks were recorded for a one-meter resonant cavity with CESR cross-sectional geometry. The squares of the frequencies f^2 , accompanied by their corresponding harmonic numbers n^2 , were fit to the hyperbolic form of Eq. 9 ($f^2 = an^2 + b$). a , the coefficient of n^2 , was solved for the length L and returned a value of 1.015m. The square root of b , corresponding to the cutoff frequency f_c , was 1.888 GHz. Based on the value of L with respect to the actual simulation length, this value for f_c is taken to be within a 1.5% margin of error.

PHASE SHIFT MEASUREMENTS

To observe small phase shifts in the physical waveguide, two pipes were connected with a small gap (as described in Section II-A) through which a plastic strip could be inserted. Metal blocks were added to both ends of the pipe as perturbations to increase reflections. (Nevertheless, reflections still would have occurred without the metal blocks - they cannot be avoided with the equipment used in this experiment.) The Lexan plastic, like the low-density cold electron plasma, behaves as a linear dielectric under the experimental conditions.

To produce a phase shift measurement, TE-waves were transmitted through the pipe (without the dielectric) and

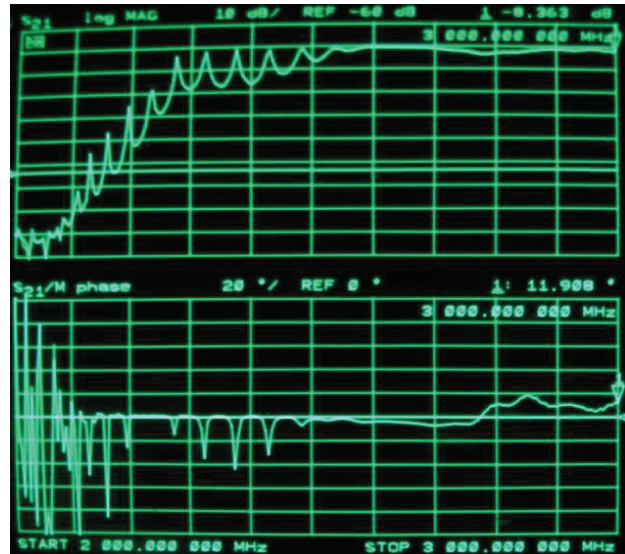


Figure 3: Network analyzer data for the phase shifts caused by a Lexan plastic dielectric in the physical conductor. The amplitude for each frequency is shown on top at 10dBm per division; the corresponding phase shifts are shown on the bottom at 20° per division.

measured by the network analyzer. The frequency was swept between two and three gigahertz. The phase shift at each frequency value was recorded in the analyzer’s memory. The dielectric was then added, and the analyzer displayed the difference between the dielectric-effected phase shift data and the stored data. The result, as shown on the bottom half of Fig. 3, was a plot of $\Delta\Phi$ versus frequency.

The top half of Fig. 3 plots amplitude versus frequency, similar to Fig. 1. The cutoff is less abrupt in this distribution, most likely due to the presence of the metal perturbations. The analyzer recorded background noise in the first division (from 2GHz to roughly 2.1GHz); hence the erratic data for $\Delta\Phi$ versus frequency in that range. Note, however, that spikes in phase shift appear at about the same frequencies as peaks in the amplitude distribution. This is indicative of greater phase shifts at resonant harmonics, as predicted.

It is also apparent that the effect of the dielectric on the signal’s phase is not the same for all frequencies. Most notably, the harmonic at ≈ 2.23 GHz (where a peak in amplitude is recorded on the top half) exhibited no noticeable phase shift from the pipe without the dielectric.

The simulation of a particle beam or even a time-varying EC was beyond the scope of the code used for these simulations, so all phase shifts were calculated based on data from an EC-containing pipe as compared to an empty pipe with all other features the same. For phase comparison, the apex-to-apex potential difference was recorded for each time step at the end of the pipe opposite the current source. For every phase comparison, these two voltage functions were essentially the same for the EC-filled pipe

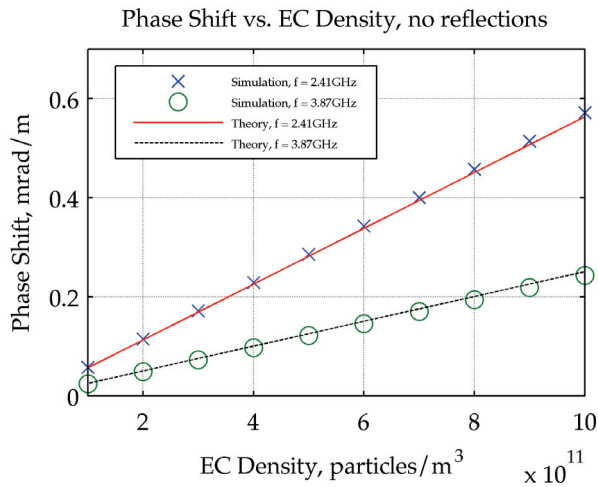


Figure 4: Phase shift data from reflection-free simulations against values predicted by Eq. 11. Electron densities are typical of those seen in CESR.

and the empty pipe (except for a small phase shift). Since these functions were essentially sinusoids at the carrier frequency, the following method could be employed to derive the phase shift $\Delta\Phi$.

Both sets of data were normalized by dividing their respective quantities by $\sqrt{2}$ times the RMS amplitude. For normalized sinusoids that differ by a small change in phase $\Delta\Phi$, the difference between them can be expressed as follows:

$$\begin{aligned} & \sin(\omega t + \Delta\Phi) - \sin(\omega t) \\ &= 2\sin\left(\frac{\Delta\Phi}{2}\right)\cos\left(\frac{2\omega t + \Delta\Phi}{2}\right) \\ &\approx \Delta\Phi\cos\left(\frac{2\omega t + \Delta\Phi}{2}\right) \end{aligned} \quad (4)$$

Thus, small phase shifts are approximately equal to $\sqrt{2}$ times the RMS of the difference between corresponding values in the two normalized sets of data.

All simulations used for phase-shift data were conducted with 0.5m CESR pipes. Drawing upon Eq. 4, the formula for the plasma frequency $\omega_p = 2\pi f_p$, and CESR's cutoff frequency f_c , the phase shift for a pipe without reflection is expected to be [8]

$$\Delta\Phi = \frac{n_e e^2 L}{4\pi\epsilon_0 m_e \sqrt{f^2 - f_c^2}} \quad (5)$$

for low values of $\Delta\Phi$.

As shown in Fig. 4, the phase shift data collected from the simulations for reflection-free pipes corresponded well to the theoretically-predicted values in Eq. 11. Similar success with a VORPAL-simulated pipe with a square cross-section has been reported before [8].

To test for the effects of reflections, the simulations were altered to include two protruding conductors. The protrusions were slabs in the transverse plane, extending from the bottom to one centimeter above the apex of the lower

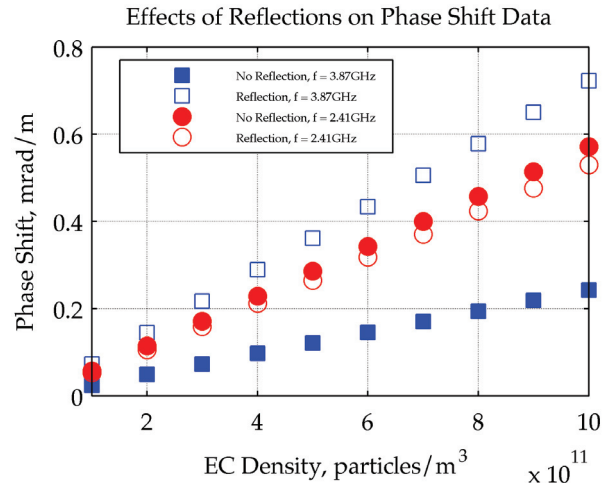


Figure 5: Phase shift data from simulations with and without reflections.

arc. They were spaced 0.4 meters apart, and the frequencies (2.41GHz and 3.87GHz, the same as the above simulation) were chosen to be the resonant harmonics ($n = 4$ and $n = 9$, respectively) of a 0.4 meter resonant cavity in order to maximize reflections. As evidence that reflections were in fact occurring between the protrusions, the energy flux (not shown) fell periodically below zero (positive flux points away from the source current), whereas the flux at the end opposite the source was always positive.

Fig. 5 shows the results. The solid shapes represent the data for no reflections and are the same data that appear in Fig. 4. The open shapes represent the phase shifts in the presence of reflection. In all cases the phase advance appears to increase in direct proportion to EC density, which is consistent with Eq. 11. The nature of the overall change in phase shift due to reflections, however, is unclear. Although we expected reflections to greatly increase the phase shift in all cases, $\Delta\Phi$ actually decreased a bit for $f = 2.41\text{GHz}$ ($n = 4$). Nevertheless, these results do not necessarily conflict with the physical data in Fig. 3, which suggests that $\Delta\Phi$ is liable to vary significantly with frequency.

DISCUSSION AND CONCLUSION

The TE-wave transmission technique requires an accurate measure of phase shift in order to successfully predict the spacial average EC density. If beam pipe reflections are capable of significantly changing the average phase advance of a TE signal, their effects must be accounted for. The results from both the physical experiments and simulations have shown that subjecting a waveguide transmission to reflections can have a major effect on phase shift, in one case causing more than a twofold increase.

The nature of the effect of reflections, however, is poorly understood. The data shown in Figs. 3 and 5 suggest that

phase shift can be greatly altered at resonant frequencies, but that this is not always the case. Further work is needed to better characterize these effects. In particular, simulations should be run on a spectrum of frequencies beginning at the cutoff to create a distribution function. Such distributions should be obtained for different varieties of reflection-generating perturbations.

The VORPAL code used for simulations with CESR beam pipe geometry has been shown to accurately portray physical systems according to waveguide theory. Although it has some limitations, in particular the short time frame of its simulations, it will be a valuable tool in future experiments.

ACKNOWLEDGEMENT

This research was supported by NSF grants PHY-0849885 and PHY-0734867, as well as DOE grant DE-FC02-08ER41538.

REFERENCES

- [1] T. Kroyer, F. Caspers, W. Höfle, M. M. Jimenez, M.-F. Malo, J. Tückmantel, and T. U. Wien. "Unexpected results on microwave waveguide mode transmission measurements in the SPS beam pipe." *Proceedings of the 31st ICFA Beam Dynamics Workshop: Electron Cloud Effects (ECLLOUD04), Napa, California 2004*, CERN Report No. CERN-2005-001, 2004
- [2] T. Kroyer, F. Caspers, and E. Mahner. "The CERN SPS experiment on microwave transmission through the beam pipe." *Proceedings of the 2005 Particle Accelerator Conference, Knoxville TN*.
- [3] S. De Santis, J.M. Byrd, F. Caspers, A. Krasnykh, T. Kroyer, M.T.F. Pivi, and K.G. Sonnad, Phys. Rev. Lett. 100, 094801 (2008)
- [4] C. Nieter and J. R. Cary. "VORPAL: a versatile plasma simulation code." J. Comp. Phys. 196, 448 (2004)
- [5] K. Yee. "Numerical solution of initial boundary value problems involving Maxwell's equations in isotropic media." IEEE Transactions on Antennas and Propagation, AP-14, 302 (1966)
- [6] J. P. Boris. "Relativistic plasma simulation-optimization of a hybrid code." Proc. Fourth Conf. Num. Sim. Plasmas, Naval Res. Lab, page 3 (1970)
- [7] J. Berenger. "A perfectly matched layer for the absorption of electromagnetic waves." Journal of Computational Physics 114, 185 (1994)
- [8] K. Sonnad, M. Furman, S. Veitzer, P. Stoltz, and J. Cary. "Simulation and analysis of microwave transmission through an electron cloud: a comparison of results." *Proceedings of PAC07, Albuquerque, NM* (2007)